Determination of photothermal conversion efficiency of graphene and graphene oxide through an integrating sphere method

Ol. S. Savchuk, J.J. Carvajal, J. Massons, M. Aguiló, F. Díaz*

Physics and Crystallography of Materials and Nanomaterials (FiCMA-FiCNA) and EMaS, Universitat Rovira i Virgili (URV), Marcel·lí Domingo 1, E-43007 Tarragona, Spain

Abstract: We report a new method for the determination of photothermal conversion efficiency of photothermal agents, based on the use of an integrating sphere. We validated this method by comparing the photothermal conversion efficiency of Au nanorods calculated by this method and by the more conventional time constant method. Then, we applied this method to determine the photothermal conversion efficiency of graphene and graphene oxide nanosheets dispersions in dimethylformamide and water, respectively, finding out that they are excellent photothermal agents with photothermal conversion efficiencies among the highest reported up to now. We also analyzed the influence of the concentration of the materials, and the wavelength and power of irradiation in the temperature increase that can be achieved with them, finding out that they can be used, for instance, in cancer treatment through hyperthermia procedures with reduced costs when compared to other photothermal agents.

1. Introduction

Heat can be used as an instrument to increase death rate in cells, useful to treat diseases as cancer, for instance [1]. Increasing the temperature of biological molecules above the limit of 39 ºC induces chemical reactions leading to unwanted products that damage cells and tissues (denaturation) in performing their functions, and finally at a temperature above 48 ºC necrosis is induced. Thus, if controlled, heat may be used to treat abnormal cells, such cancer cells, through hyperthermia treatment. However, heat also affects negatively to health tissues. Thus, predicting and controlling the temperature distribution in a body region during hyperthermia treatment is mandatory [2].

Conventional methods of temperature promotion in abnormal cells can be classified by: (i) external heating mainly used for superficial tumors, induced by radiofrequency [3], microwave [4] or ultrasounds [5]; and (ii) internal heating for non-

*corresponding author: Joan J. Carvajal, Physics and Crystallography of Materials and Nanomaterials (FiCMA-FiCNA) and EMaS, UniversitatRoviraiVirgili (URV), Marcel·lí Domingo 1, E-43007 Tarragona, Spain
Email address: joanjosep.carvajal@urv.cat

superficial tumors using electrodes or antennas located very close to the tumor [6, 7]. However, these methods face great difficulties deriving mainly from the complex nature of organs and tissues, and undesirable hyperthermia effects induced in surrounding tissues.

To avoid the non-specific heating of surrounding tissues, especially in the case of non-superficial tumor treatments, laser irradiation at near-infrared (NIR) frequencies has been explored [8]. This radiation is less absorbed by biological tissues, thus, penetration depths of several centimeters in biological tissues can be achieved using this radiation [9-11].To use this kind of radiation in an effective way, the use of photothermal agents that can convert the NIR light energy into thermal energy is indispensable. Photothermal agents mainly include: (i) metal plasmonic nanostructures (Au nanostructures [12], Pd-based nanosheets[13] and Ge nanoparticles [14]); (ii) organic compounds (polyaniline [15], polypyrrole [16], dopamine-melanin [17], polymers [18]); (iii) nanoparticles with ferromagnetic properties alone, or combined with good absorbers in the NIR region (FePt [19], $ZnFe_2O_4$–reduced graphene oxide [20], Fe_3O_4@polylactic acid coated with graphene oxide [21], WO_3nanorods [22]); and (iv) semiconductor nanoparticles ($Cu_{2-x}Se$ [23], CuS [24]).

Among these photothermal agents, Au nanostructures have the ability to accumulate within a solid tumor in the body [12], and since their surface plasmon resonance can be tuned within a broad range of wavelengths from the visible to the NIR [12], Au nanostructures can be tailored for particular hyperthermia treatments. However, despite the excellent photothermal conversion efficiency and great physical properties, Au nanostructures have bad photostability after a long period of laser irradiation [25], and new photothermal agents have been developed to overcome these problems. However, their photothermal conversion efficiency is low [23-25], which implies the necessity of using a higher concentration of nanoparticles or a higher power density of the laser irradiation to generate hyperthermia. Another problem is that the size of these photothermal agents is considerably big, which reduces the time of blood stream circulation before their deposition in blood vessels [26]. From another side, although the use of magnetic nanoparticles allows having contrast agents for tomography and magnetic resonance imaging [19-22], the powerful femtosecond laser irradiation needed to excite them and increase the temperature of biological tissues, generates microbubbles that cause irreversible damages [19].

Thus, an ideal photothermal agent should meet several requirements, as suitable nanosize and uniform shape, good dispersability in aqueous solution or biological compatible fluids, large NIR absorption cross-section, high photostability and low cytotoxicity in living systems.

Graphene-based materials have emerged as promising photothermal agents for photothermal therapy especially due to their high absorption cross-sections in the NIR that can be combined with the ability to modify chemically those materials to use them also as drug loaders [27]. Photothermal therapy based on graphene materials has been extensively investigated for cancer therapy [28-33], and antibacterial treatment [27]. Also, magnetic nanoparticles that acted as good contrast agents for magnetic resonance have been used together with graphene-based materials [21], in which the photothermal effect could be enhanced by applying an external magnetic field [34]. On the other hand graphene (G) can be functionalized with fluorescent dyes or up-conversion nanoparticles that can serve as imaging probes for photothermal therapy [35]. Moreover, graphene-based magneto-plasmonic nanocomposites have been developed for simultaneous enhancement of the NIR absorption and multimodal imaging guided cancer therapy [34]. This is especially important when operating in the so-called biological windows [36] corresponding to the 650-950 and 1000-1350 nm spectral ranges, where tissue scattering and absorption are minimized, and where graphene-based materials can operate efficiently [37].

Despite the large number of studies about the use of graphene-based materials on photothermal therapy, there are no reports on determining the photothermal efficiency of these graphene-based materials with the objective of predicting and controlling the temperatures that can be generated with them.

In the present work we developed a fast and effective method for determining the efficiency of the heat production after laser illumination based on the use of an integrating sphere. We validated it by comparing the photothermal efficiency of gold nanorods measured by using the integrating sphere and the time constant method [38], well stablished in the literature. Finally, we applied this method to determine the photothermal efficiency of graphene (G) and graphene oxide (GO), and analyzed the dependence of their heat converting capacity on the material concentration in the solvent, the laser power irradiation and the wavelength of the laser with which those photothermal agents are illuminated.

2. Experimental Section

2.1 Photothermal agents

A GO colloidal suspension dispersed in distilled water, with flake sizes between 300 and 700 nm and 60% of the sample with a thickness of 1 atomic layer, provided by Graphene Market and a G colloidal suspension dispersed in dimethylformamide (DMF), with flake sizes between 150 and 3000 nm and 60% of the sample with a thickness of 1 atomic layer, provided by Granph Nanotech, were used as photothermal agents. DMF, although not being a biological compatible fluid, was used since it has a surface tension similar to the surface energy of G, and thus prevent G nanosheets from aggregation. The colloids were diluted for obtaining different concentrations, from 0.5 to 5 g/l in the case of GO and from 0.05 to 1 g/l in the case of G. Since G has a larger absorption cross-section in the NIR, we reduced its concentration to obtain comparable results with those obtained when using GO.

Citrate-caped gold nanorods with an axial diameter of 25 nm, a length of 50 nm, and a concentration of 150 μg/ml were provided by Strem Chemicals.

2.2 Absorption measurements

The optical absorption measurements of the GO, G and Au nanorods in solutions, with a concentration of 1 g/l, 1 g/l and 150 μg/ml, respectively, were recorded using a Varian Cary 500 Scan spectrometer. This spectrometer has two monochromators with a 1200 lines/mm grating for the UV/VIS region and a 300 lines/mm grating in the NIR region. The optical sources used were a deuterium lamp and a quartz halogen lamp in the zone of visible and infrared. The detectors were a photomultiplier tube in UV/VIS region (175 – 850 nm) and a lead sulfide diode in the IR region (850 – 3300 nm).

2.3 Photothermal conversion efficiency determined from the time constant

For photothermal conversion measurements, 0.3 ml of samples were introduced in a glass cuvette (Helma Analytics) with dimensions 2×1 cm. Solutions were irradiated with a Lumics fiber-coupled diode laser emitting at 808 and 980 nm in order to study the wavelength dependent photothermal conversion. In the case of Au nanorods, they were irradiated with a 650 nm diode laser. The laser beam was focused on the cuvette with a

collimating lens, allowing a beam diameter of 5 mm on the sample. The temperature evolution was recorded by a digital multimeter connected to a small Pt-100 thermo-resistor located inside of the cuvette. After around 10 min of irradiation, the sample reached the thermal equilibrium, and thus the maximum temperature for a particular laser power irradiation. After that, laser irradiation was switched off for allowing the sample to cool down to the room temperature while data were recorded in the cooling cycle.

2.4 Photothermal conversion efficiency using an integrating sphere

For photothermal conversion efficiency using an integrating sphere the glass cuvette containing the sample (GO in water with a concentration 1 g/l or G in DMF with a concentration 1 g/l) was placed inside the integrating sphere, perpendicular to the laser irradiation provided by the fiber-coupled diode laser emitting at 808 and 980 nm, with a power of 200 mW. The laser from the fiber tip was collimated with a spot size of 5 mm in diameter on the sample. A baffle was introduced in the integrating sphere, between the sample and the detector, in order to prevent the direct reflections from the sample to the detector. The signal was collected using a powermeter Ophir Nova II. An scheme of the experimental setup used for these measurements is provided in Figure 1.

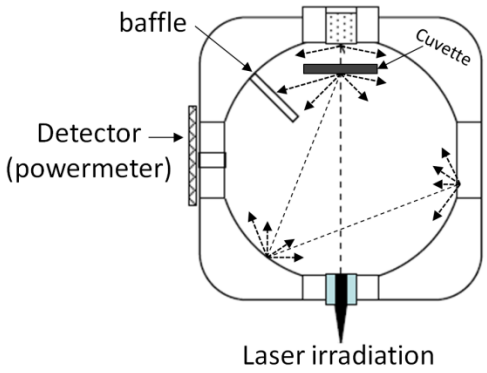

Figure 1. (a) Scheme of the setup for photothermal conversion efficiency measurements.

3. Results and Discussion

Figure 2(a) shows the room temperature visible-NIR absorbance spectra of 1 g/l GO and 1g/l G nanosheets colloidal suspensions in water and dimethylformamide (DMF),

respectively. In the case of GO, the absorbance falls almost exponentially from the UV region to the NIR region. Instead, G shows an almost constant absorbance all over the visible and NIR regions, higher than the theoretical one that would be expected for monolayer graphene [39], but similar to that reported for other graphene samples [40]. The inset in the figure shows the absorption of GO and G in the so-called first biological window (650-1000 nm) [36] and we can observe that the absorption of GO decrease slightly in this range of wavelengths, while that of G is almost constant.

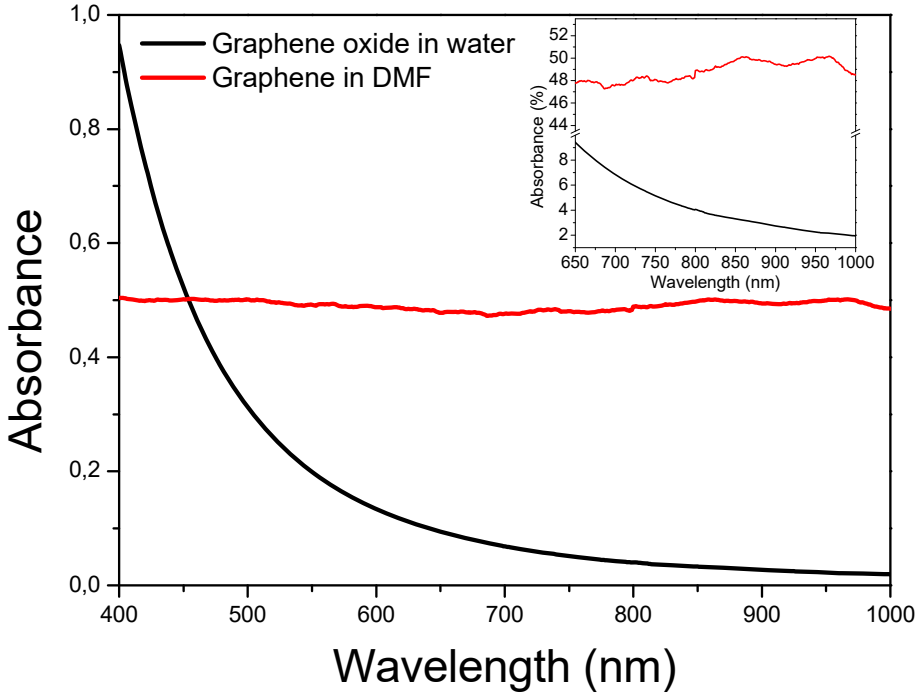

Figure 2. Absorption spectra of GO in water and G in DMF in the visible and NIR ranges. Inset shows a magnification of the curves in the 650-1000 nm range, coinciding with one of the biological windows.

We focused our attention on two particular wavelengths that are often used to illuminate photothermal agents, 808 and 980 nm, since they also constitute two consolidated laser wavelength technologies. GO shows an absorbance of 4% at 808 nm that is reduced to 2%, at 980 nm. Instead, G shows an absorbance one order the magnitude higher at 808 nm (48%), and it is maintained at 980 nm (49%).

We compared the temperature increase of the GO and G dispersions in water and DMF, respectively, at two different irradiation wavelengths. Figure 3(a) shows the results of the irradiation with 980 nm. It should be noted that after approximately 10 minutes of irradiation time, the system reached the steady state (see Figure 3(a)), when the heat

produced by the material is compensated by the heat irradiated to the environment. The temperature increase for GO in water is about 3 ºC, however for G in DMF the temperature increase is 4 times higher, around 12 ºC. At 808 nm, the temperature increase for GO in water is about 4 ºC, higher than that obtained at 980 nm due to the higher absorption of GO at this wavelength, while that of G in DMF is 15 ºC, as can be seen in Figure 3(b).

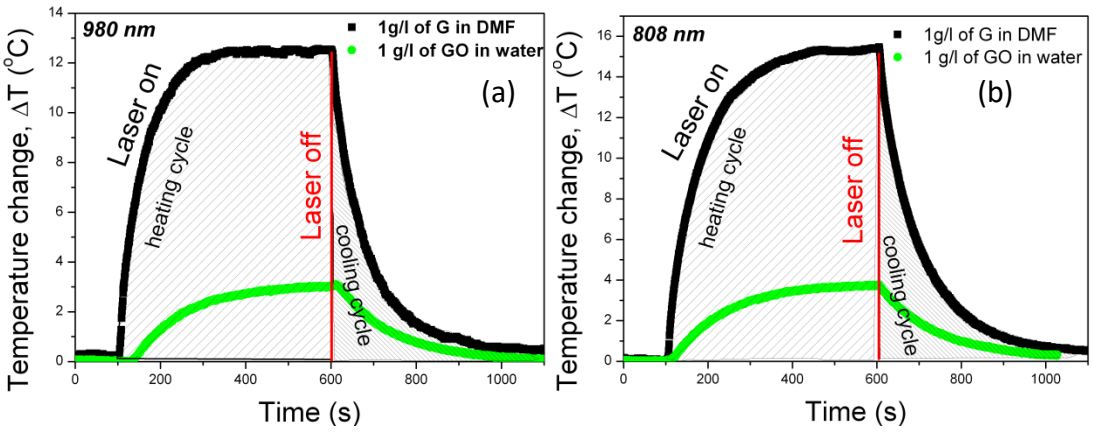

Figure 3. (a) Temperature profile of the G and GO under the same conditions with 980 nm irradiation wavelength; (b) Temperature profile of G and GO at 808 nm irradiation wavelength.

We also investigated the influence of the GO and G concentrations and the power of the laser irradiation on the temperature that can be achieved in the liquid dispersions. The results of these analysis for GO in water are shown in Figure 4(a). As can be seen, the temperature increases almost linearly as the power of the laser increases. When illuminated at 980 nm, the temperature increase ranged from 4 ºC at an irradiation power of 200 mW to 14 ºC at the highest irradiation power (800 mW) for a concentration of 5 g/l of GO in water. If we focus our attention of the GO concentration on water, the temperature increase varied from 2 ºC for a concentration of 0.5 g/l to 7.5 ºC for a concentration of 5 g/l, while keeping the irradiation power at 400 mW. When illuminated at 808 nm, the temperature increase that can be achieved was higher, as expected from the higher absorption of GO at this wavelength. It ranged from 3 ºC for an irradiation power of 100 mW to 22 ºC for an irradiation power of 800 mW for a concentration of 5 g/l. The increase of temperature depending on the concentration of GO in water also changed, achieving 2.5 ºC for a concentration of 0.5 g/l and 12 ºC for a concentration of 5 g/l, while keeping the irradiation power at 400 mW in both cases.

In the case of G nanosheets dispersed in DMF, the results are shown in Figure 4(b). The results are similar for both wavelengths, although higher at 808 nm, changing from around 6-9 ºC at an irradiation power of 100 mW to 45-54 ºC at 800 mW. The concentration dependence of the heat produced, changed from 3-4 ºC for a concentration of 0.1 g/l to 13-15 ºC for a concentration of 1 g/l, at an irradiation power of 200 mW. Note, however, that the concentration and power of the laser in the case of G in DMF had to be reduced in order to maintain the range of temperature variation achieved previously on GO.

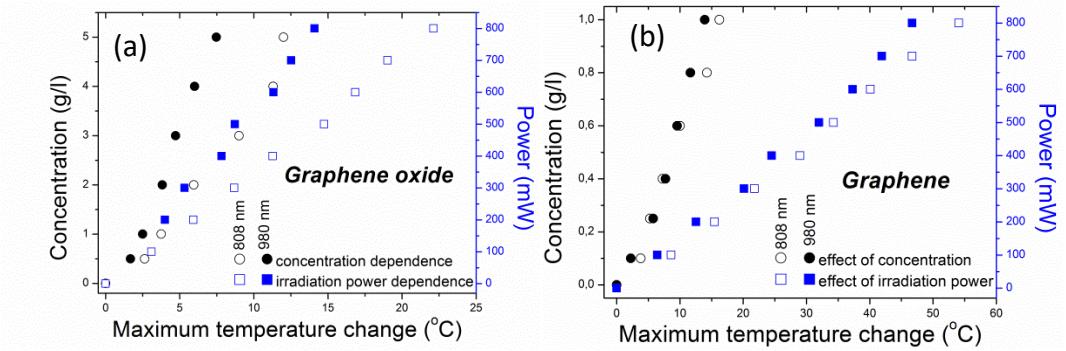

Figure 4.Temperature change under 980 and 808 nm laser irradiation at different concentrations and different irradiation powers of (a) GOnanosheets dispersed in water, and (b) G nanosheets dispersed in DMF.

For the G dispersion in DMF, the temperature change values that can be achieved under these conditions are more or less double of those that can be achieved when using GO in water, using much less quantity of material in the solvent. This can be explained by the higher absorption of G. These results show that just by changing the wavelength of irradiation, the applied irradiation power or the concentration of the photothermal agent, we can vary the heat produced by G or GO, achieving an appropriate value for a particular application. For instance, it has been shown that cancer cells can be killed after maintenance at 42 ºC for 15 – 60 min or over 50 ºC for 4 – 6 min [41]. These conditions can be achieved by using a concentration of GO of 5 g/l in water, illuminated at 808 nm with a power of 800 mW, or a concentration G of 1 g/l in DMF, illuminated at 808 nm with a power of 400 mW.

We determined the photothermal efficiency of G and GO by using an integrating sphere. In the scheme presented in Figure 5, we show the basic processes of interaction of light with a photothermal agent. The incident light (0) can be: (1) absorbed by the material; (2) absorbed by the cuvette and the solvent; (3) scattered and reflected from the

wall of the cuvette or the surface of material; (4) the non-reflected and non-absorbed light can be transmitted.

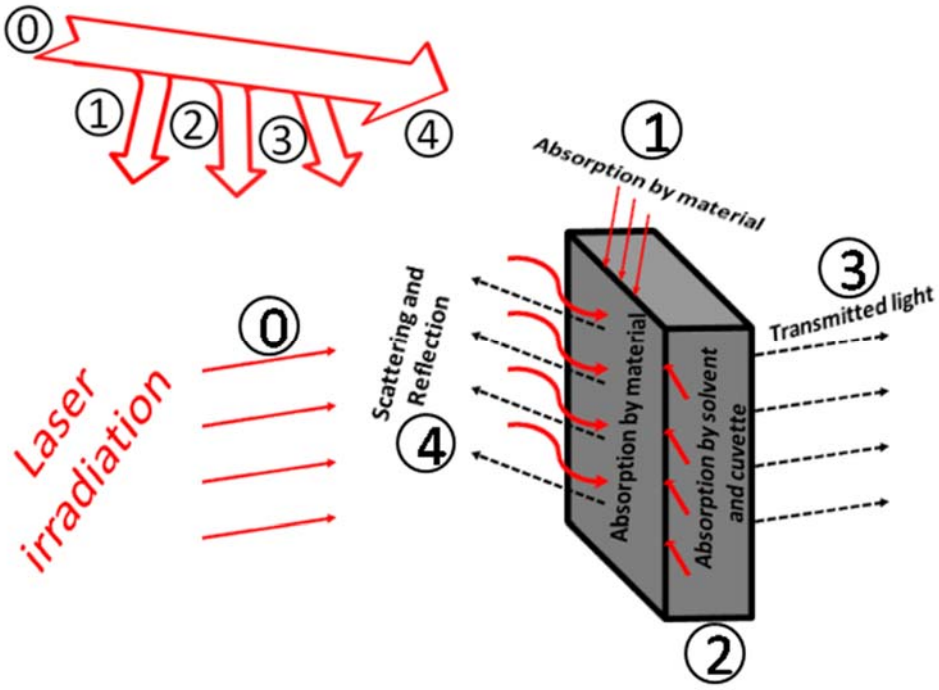

Figure 5. Scheme showing the interaction of the light with the material (G and GO in this case) when using an integrating sphere.

In our calculations we have assumed that all the light absorbed by the photothermal agent is transformed to heat. Taking into account that with the integrating sphere we are able to measure reflected, scattered and transmitted light, the photothermal conversion efficiency can be calculated by the following equation:

$$\eta = \frac{P_{heat}}{P_{inc}} = \frac{P_{blank} - P_{sample}}{P_{empty} - P_{sample}} \quad (1)$$

where P_{empty} define the power that was measured in the integrating sphere without sample, P_{sample} is the power that was measured when the sample was inside of the sphere, P_{blank} is the power measured when only the solvent was present in the cuvette inside of the integrating sphere.

The photothermal efficiencies calculated by this method for G and GO after illumination at 808 and 980 nm are listed in Table 1, together with the parameters used to determine them. The results show that the photothermal efficiency of G in DMF is

around 63-67 (± 5) %, and quite similar at the two wavelengths analyzed. However, the photothermal efficiency of GO in water depends on the wavelength used to irradiate the sample, being higher at 808 nm, as expected, since the optical absorption of GO is higher at this wavelength.

Table 1. Data of calculated photothermal efficiency using the integrating sphere.

Material	**Wavelength of irradiation (nm)**	**Incident power (mW)**	**P_{empty} (mW)**	**P_{blank} (mW)**	**P_{sample} (mW)**	**Efficiency (%)**
G	808	200	6,2	4,37	0,58	67 ± 5
GO	808	200	6,2	4,38	1,9	58± 5
G	980	200	7,82	5,32	1	63 ± 5
GO	980	200	7,82	4,07	2,02	35 ± 5

Table 2. Photothermal conversion efficiency of G and GO compared with other photothermal materials reported in the literature.

Material	**Irradiation wavelength (nm)**	**Incident power (W)**	**Method**	**Efficiency (%)**	**Ref.**
Hollow Au-Ag alloy nanourchins	808	1	Time constant	80.4	**[12]**
Au nanorods	815	0.151	Time constant	61	**[42]**
Au/AuS nanoshells	815	0.161	Time constant	59	**[42]**
$Cu_{7.2}S_4$ nanoparticles	980	0.29	Time constant	56.7	**[43]**
Au nanorods	808	2	Time constant	50	**[44]**
Dopamine-melanin coloidal nanospheres	808	2	Time constant	40	**[17]**
Biodegradable Au nanovesicles	808	1	Time constant	37	**[45]**
Au/SiO_2 nanoshells	815	0.163	Time constant	34	**[42]**
FePt nanoparticles	800	1 μJ per pulse	$\frac{P_{converted\ to\ heat}}{P_{excitation}}$	30	**[19]**
Cu_9S_5 nanoparticles	980	0.51	Time constant	25.7	**[23]**
Au nanoshell	808	2	Time constant	25	**[44]**
$Cu_{2-x}Se$ nanoparticles	800	2	Time constant	22	**[24]**
Au nanorods	808	1	Time constant	22	**[45]**
Au nanoshells	808	1	Time constant	18	**[45]**

The high values of photothermal efficiencies we determined for G and GO are among the highest reported for photothermal agents, as can be seen in Table 2 where we included data of photothermal efficiencies of other photothermal materials reported in the

literature. Especially when illuminated at 808 nm, they are higher than those reported for Au nanostructures [7, 10, 46], semiconductors materials [47, 16, 17]; polymer nanostructures [45, 48], or nanoparticles with ferromagnetic properties [13]. Only Au-Ag alloy urchin shaped nanostructures show a higher efficiency of ~80 % [12], but G and GO can be produced at a more competitive price when compared to this alloy. When irradiated with a laser beam with emission at 980 nm, while G is still the most efficient photothermal agent, other materials like $Cu_{7.2}S_4$ nanocrystals show a higher photothermal conversion efficiency [43] than GO. Still, however, GO is one of the materials with the highest photothermal conversion efficiency at that wavelength.

This higher photothermal conversion efficiency of G and GO as photothermal agents is important, since they can be used to combat cancerous cells but using a lower concentration of material, a shorter irradiation time and a lower irradiation power, which apart from being more cost effective, is safer for the healthy tissues of the body. If we compare the results obtained for G and GO, despite the photothermal efficiency determined for G is higher, it is not dispersible in water, or any other suitable solvents for biological applications, unless a chemical functionalization process is developed that, of course, will affect to its light absorption properties, and thus, will modify its photothermal conversion efficiency. From another side, GO although having lower photothermal efficiency than G, since it can form hydrogen bonds between the polar functional groups present on its surface and the water molecules surrounding, it and can form a stable colloidal suspension, thus, having advantages for potential biomedical applications. In this context, it is worth to mention that the attachment of polyethylene glycol (PEG) to graphene derivatives increased substantially the optical absorption of these materials, increasing substantially their photothermal conversion efficiency [28, 30, 31, 33]. In front of other photothermal agents, such as Au nanostructures, a part from the higher photothermal efficiency, G and GO have an additional advantage, since Au nanoparticles tend to change their shape when illuminated with a high laser power, thus modifying their plasmonic resonances [49] which will decrease significantly their photothermal efficiency at that particular wavelength.

Table 3. Comparison of the photothermal conversion data reported in the literature for different graphene-based materials for an irradiation wavelength of 808 nm.

Material	**Concentration ($g\ l^{-1}$)**	**Power density ($W\ cm^{-2}$)**	**Absorbance**	**ΔT_{max} (ºC)**	**Time (s)**	**Reference**

PEGylated nano G	0.5	2	0.5	35	180	[28]
Nano reduced GO	0.02	0.6	19	27	480	[29]
Nano GO	0.02	0.6	2	12	420	[29]
PEGylated nano reduced GO	0.01	1	0.2	29	300	[30]
PEGylated reduced GO	0.01	1	0.22	29	300	[30]
PEGylated nano GO	0.01	1	0.07	15	300	[30]
PEGylated GO nanoribbons	0.001	7.5	0.55*	34	600	[31]
PEGylated reduced GO	0.001	7.5	0.22*	20	600	[31]
GO nanoribbons	0.001	7.5	0.05*	5	600	[31]
Glucose reduced GO + Fe catalyst	0.1	7.5	0.32#	38	120	[32]
Hydrazine reduced GO	0.1	7.5	0.32#	45	120	[32]
GO	0.1	7.5	0.02#	10	120	[32]
PEGylated GO nanomesh	0.01	0.1	1.1	30	460	[33]
PEGylated reduced GO nanoplates	0.01	0.1	0.39	16	460	[33]
PEGylated reduced GO	0.01	0.1	0.42	15	460	[33]
GO nanomesh	0.01	0.1	0.03	5	460	[33]
GO	1	1	0.05	4	400	This work
G	1	1	0.48	15	400	This work

* The absorbance has been determined with a concentration of 1 g l^{-1}.

The absorbance has been determined with a concentration of 0.5 g l^{-1}.

When comparing the photothermal conversion efficiency of graphene-based materials reported in the literature with the results presented in this manuscript, what we observed is that in general the photothermal conversion efficiency reported in the literature is presented just as a temperature evolution profile, similar to that shown here in Figure 3. This makes difficult the task of comparing our results with those previously reported. However, we listed the available data in the literature with the idea to stablish some comparisons between the results reported previously and those achieved in the present paper. Table 3 shows this comparison.

As can be seen in the table, materials were excited at different laser power densities, different concentrations were used, and even absorbances are plotted in

different scales without indicating if they are in a 1 scale or in %. This adds some difficulties to establish these comparisons. However, some generalizations can be extracted from these data. First, GO is the graphene derivative showing a smaller photothermal conversion, with temperature increments of the order of 4-5 ºC, even in the form of nanomeshes or nanoribbons. From another side, it is clear that reduced GO shows a higher photothermal conversion that can multiply by 9 the temperature increment achieved by GO. Finally, another important tendency is that the materials tending to show the maximum photothermal conversion are those that are linked to polyethylene glycol (PEG) that also show the highest absorbance, indicating a synergistic effect between the graphene derivative and PEG. It should also be noted that the same material in different sizes, PEGylated nano reduced GO vs. PEGylated reduced GO for instance, tend to show the same photothermal conversion, indicating that the lateral size of the graphene-derivative flakes does not have an influence on the photothermal properties of the material. Thus, apparently from the data reported, it seems that the photothermal conversion is linked to the absorbance of a particular material: the higher the absorbance, the higher the photothermal conversion. Note also, that in this comparison we did not include the composite materials of graphene or graphene derivatives with other inorganic and organic materials developed also for photothermal treatments, since it would difficult even more the task of establishing general tendencies.

To validate this new method for the determination of the photothermal efficiency of G and GO, we calculated the phototermal efficiency of Au nanorods by using the integrating sphere, and compared the photothermal efficiency obtained by this method with that obtained using the time constant method [44], a method well established for this purpose. Figure 6 (a) shows the absorption spectra of these Au nanorods, with 2 absorption bands located at 525 and 650 nm, corresponding to the transversal and longitudinal plasmonic resonances. We used this last wavelength, with a power of 200 mW, to illuminate the Au nanorods and determine their photothermal efficiency.

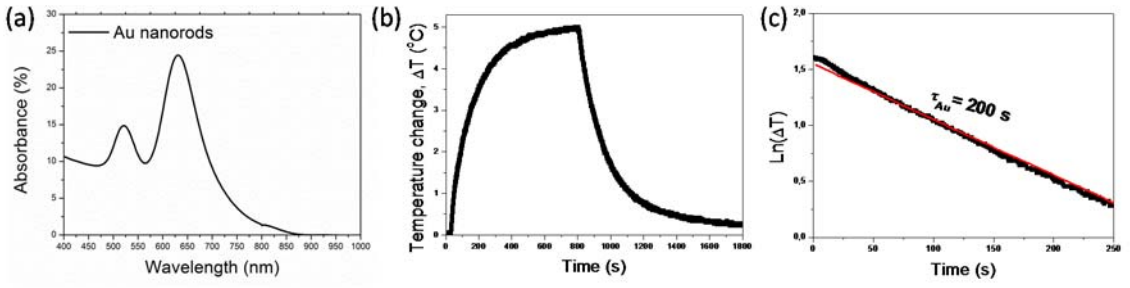

Figure 6. (a) Absorption spectrum of Au nanorods, 25 nm in diameter and 50 nm in length. (b) Temperature profile generated by Au nanorods being excited at 650 nm with a diode laser. (c) Time constant for heat transfer of the Au nanorods by applying the natural logarithm of temperature change versus time data, which is obtained from the cooling cycle shown in panel (b).

To apply the time constant method, we take into account that the time evolution of the temperature after the laser was switched off can be described by equation (cooling cycle in Fig. 6b):

$$\Delta T = (T_{max} - T_{amb})\, exp\left(-\frac{t}{\tau}\right) \quad (2)$$

where ΔT is the change of temperature; T_{max} is the maximum temperature reached by the sample, T_{amb} is the ambient temperature of the surroundings; t is time; and τ is the thermal time constant. This thermal time constant can be calculated by:

$$\tau = \frac{\sum_i m_i c_{pi}}{hA} \quad (3)$$

Here, h is the convective heat transfer coefficient, A is the external area of the cuvette and m_i and c_{pi} are the mass and specific heat of each element of the system, respectively (glass cuvette, solvent, heating material). The fitting of the temperature evolution data as a function of time to equation (2) allows determining τ from which we can determine the heat transfer coefficient h in equation (3). Finally, the thermal conversion efficiency was calculated using the equation proposed by Roper as following [38]:

$$\eta = \frac{hA(T_{max} - T_{amb}) - Q_0}{I(1 - 10^{-A_\lambda})} \quad (4)$$

where Q_0 is the heat dissipated from the light absorbed by the glass cuvette and the solvent - that was determined independently, by using a glass cuvette filled with the solvent- I is the laser incident power, and A_λ is the absorbance of the material.

The photothermal efficiency calculated for Au nanorods using the integrating sphere or the time constant methods are listed in Table 4.

Table 4. Photothermal efficiency for Au nanorods calculated by two methods.

Material	Wavelength of irradiation (nm)	Incident power (mW)	Method of calculation	Efficiency (%)
Au nanorods	650	200	Integrating sphere	56 ± 5
Au nanorods	650	200	Time constant method	52 ± 5

As can be seen from the table, the values obtained by both methods are similar. Thus, the method of determining the photothermal conversion efficiency using an integrating sphere proved its expectations and can be used as another technique with more advantages than the time constant method. Also, the value of the photothermal conversion efficiency calculated by the time constant method is in a good agreement with those previously reported for Au nanorods [38].

Finally, and to show the compatibility of both methods for determining this parameter in graphene-based materials, we compared the photothermal conversion efficiency values for G and GO determined by the integrating sphere method and the time constant method. For that, we determined the time constant from the cooling cycles of the evolution of temperature with time for G and GO illuminated at 980 and 808 nm presented in Figure 3. The time constants for G and GO are shown in Figure 7. Figure 8 shows the comparison of the photoluminescence conversion efficiencies for G, GO and Au nanorods determined by both methods. As we can see in the figure, the photothermal conversion efficiencies for all the materials considered is similar, or even the same when the uncertainties are considered, independently of the determination method used. This validates the method we developed using the integrating sphere for determination of the photothermal conversion efficiency, that simplifies the procedures required for the determination of this parameter.

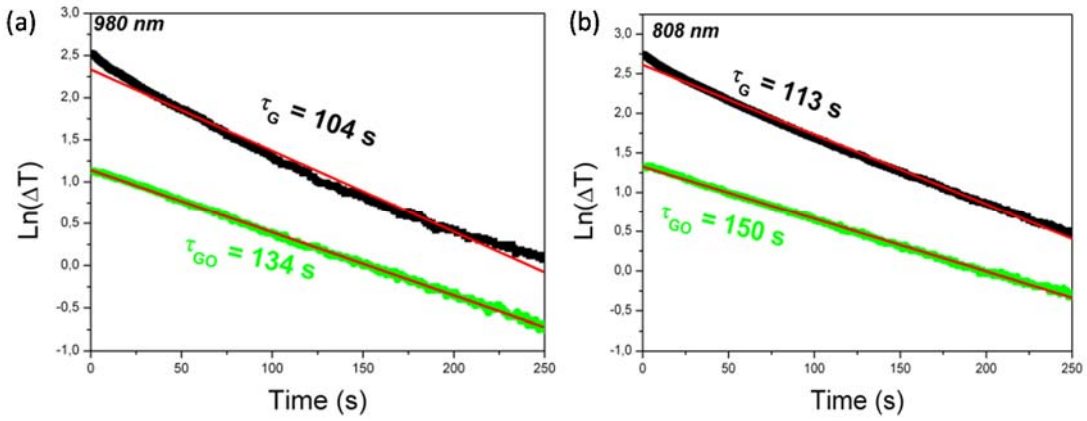

Figure 7. Time constants for heat transfer of graphene and graphene oxide by applying the natural logarithm of temperature change versus time data, which is obtained from the cooling cycles shown in Figure 3 after illumination at (a) 980 nm and (b) 808 nm.

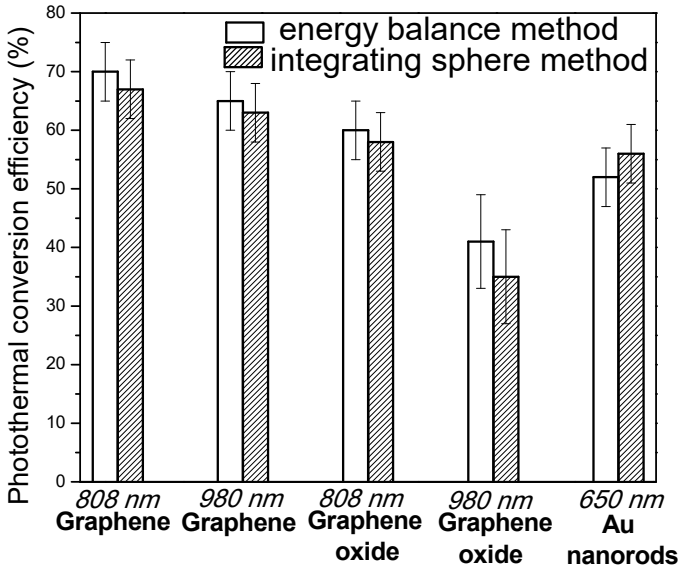

Figure 8. Comparison of the photothermal conversion efficiencies of graphene, graphene oxide and Au nanorods determined by the time constant and the integrating sphere methods.

4. Conclusion

In conclusion we developed and validated a new method for determining the photothermal efficiency of G and GO using an integrating sphere. Compared to the time constant method for determining the same parameter, the integrating sphere presents the advantage of simplicity. By applying this method we found that the photothermal efficiency of G and GO are among the highest reported for photothermal agents, which identify them as important photothermal agents for biological purposes, such as

eliminating cancer cells by hyperthermia treatments. Even, from the data reported in the literature for other graphene derivatives, if those materials are functionalized with PEG or are produced in the form of nanoribbons or nanomeshes, their photothermal conversion efficiencies might be higher. This method is not exclusive for graphene-based materials, but can also be used for any photothermal material, and will allow detecting differences in phototermal conversion efficiency when the absorbance properties of the materials are different, since the method is sensible to these changes, with the additional advantage that it is not necessary to know the optical absorbance of the material to be analyzed in advance. We also analyzed the influence of the concentration of G and GO, and the wavelength and power of irradiation in the temperature increase that can be achieved with them. The results indicate that by using a concentration of GO of 5 g/l in water illuminated at 808 nm with a power of 800 mW, or a concentration of G of 1 g/l in DMF illuminated at the same wavelength with a power of 400 mW, we can obtain the temperature increase required for cancer treatment by hyperthermia.

Acknowledgements

This work was supported by the Spanish Government under Projects No. MAT2013-47395-C4-4-R and TEC2014-55948-R, and by Catalan Authority under Project No. 2014SGR1358.Ol. A. Savchuk is supported by Catalan Government through the fellowship 2015FI_B2 00136. F. D. acknowledges additional support through the ICREA Academia awards 2010ICREA-02 for excellence in research.

References

[1] Pustovalov VK, Astafyeva LG and Fritzsche W. Selection of thermo-optical parameter of nanoparticles for achievement of their maximal thermal energy under optical irradiation. Nano Energy 2013;2:1137–1141.

[2] Lepock JR, Frey HE, Rodahl AM and Kruuv J. Thermal analysis of CHL V79 cells using differential scanning calorimetry: implications for hyperthermic cell killing and the heat shock response. J Cell Physiol 1988;137:14–24.

[3] Wust P, Hildebrandt B, Sreenivasa G, Rau B, Gellermann J, Riess H, Felix R and Schlag PM. Hyperthermia in combined treatment of cancer. Lancet Oncol 2002;3: 487–497.

[4] Jones E L, Oleson JR, Prosnitz LR, Samulski TV, Vujaskovic Z, Yu D, Sanders LL and Dewhirst MW. Randomized trial of hyperthermia and radiation for superficial tumors. J Clin Oncol 2005;23:3079–3085.

[5] Marmor JB, Pounds D, Postic TB and Hahn GM. Treatment of superficial human neoplasms by local hyperthermia induced ultrasound. Cancer 1979;43:188–197.

[6] Mulier PMJ and Hoey MF. Method and apparatus for RF ablation and hyperthermia. US patent 5807395A, 1998.

[7] Sogawa A, Inokuchi K, Sugimachi K, Kai H, Hotta T and Kawai Y. Endotract antenna device for hyperthermia. US patent 4662383A, 1987.

[8] Carrasco E, Rosal B, Sanz-Rodríguez F, de la Fuente ÁJ., Haro-Gonzalez P, Rocha U, Kumar KU, Jacinto C, Solé JG, and Jaque D. Intratumoral thermal reading during photo-thermal therapy by multifunctional fluorescent nanoparticles. Adv Funct Mater 2015;25:615–626.

[9] Chen, ZG, Zhang LS, Sun YG, Hu JQ, Wang DY. 980 nm laser-driven photovoltaic cells based on rare-earth up-converting phosphors for biomedical applications. Adv Funct Mater 2009;19:3815–3820.

[10] Chen WR, Adams RL, Carubelli R, Nordquist RE. Laser-photosensitizer assisted immunotherapy: a novel modality for cancer treatment. Cancer Lett 1997;115: 25–30.

[11] Chen WR, Adams RL, Higgins AK, Bartels KE, Nordquist RE. Photothermal effects on murine mammar tumors using indocyanine green and an 808-nm diode laser: an in vivo efficacy study. Cancer Lett 1996;98:169–173.

[12] Liu Z, Cheng L, Zhang L, Yang Z, Liu Z, Fang J. Sub-100 nm hollow Au-Ag alloy urchin-shaped nanostructure with ultrahigh density of nanotips for photothermal cancer therapy. Biomaterials 2014;35:4099-4107.

[13] Tang S, Chen M, and Zheng N. Sub-10-nm Pd nanosheets with renal clearance for efficient near-infrared photothermal cancer therapy. Small 2014;10(15):3139–3144.

[14] Yin HB, Cai HH, Cai JY, Teng JW, Yang PH. Facile solution for the syntheses of water-dispersable germanium nanoparticles and their biological applications. Materials Lett 2013;109:108-111.

[15] Zhou J, Lu Z, Zhu X, Wang X, Liao Y, Ma Z, Li F. NIR photothermal therapy using polyaniline nanoparticles. Biomaterials 2013;34:9584-9592.

[16] Zha Z, Yue X, Ren Q, and Dai Z. Uniform polypyrrole nanoparticles with high photothermal conversion efficiency for photothermal ablation of cancer cells. Adv Mater 2013;25:777–782.

[17] Liu Y, Ai K, Liu J, Deng M, He Y, and Lu L. Dopamine-melanin colloidal nanospheres: an efficient near-infrared photothermal therapeutic agent for in vivo cancer therapy. Adv Mater 2013;25:1353–1359.

[18] Xu L, Cheng L, Wang C, Peng R and Liu Z. Conjugated polymers for photothermal therapy of cancer. Polym Chem 2014;5:1573-1580.

[19] Chen CL, Kuo LR, Lee SY, Hwu YK, Chou SW, Chen CC, Chang FH, Lin KH, Tsai DH, Chen YY. Photothermal cancer therapy via femtosecond-laser-excited FePt nanoparticles. Biomaterials 2013;34:1128-1134.

[20] Akhavan O, Meidanchi A, Ghaderid E and Khoei S. Zinc ferrite spinel-graphene in magneto photothermal therapy of cancer. J Mater Chem B 2014;2:3306-3314.

[21] Li XD, Liang XL, Yue XL, Wang JR, Li CH, Deng ZJ, Jing LJ, Lin L, Qu EZ, Wang SM, Wu CL, Wu HX and Dai ZF. Imaging guided photothermal therapy using iron oxide loaded poly(lactic acid) microcapsules coated with graphene oxide. J Mater Chem B 2014;2:217.

[22] Zhou Z, Kong B, Yu C, Shi X, Wang M, Liu W, Sun Y, Zhang Y, Yang H, Yang S. Tungsten oxide nanorods: an efficient nanoplatform for tumor CT imaging and photothermal therapy. Sci Rep 2014;4:3653-3663.

[23] Tian Q, Jiang F, Zou R, Liu Q, Chen Z, Zhu M, Yang S, Wang J, Wang J and Hu J. Hydrophilic Cu_9S_5 nanocrystals: a photothermal agent with a 25.7% heat conversion efficiency for photothermal ablation of cancer cells in vivo. ACS Nano 2011;5(12):9761–9771,.

[24] Hessel CM, Pattani VP, Rasch M, Panthani MG, Koo B, Tunnell JW and Korgel BA. Copper selenide nanocrystals for photothermal therapy. Nano Lett 2011;11:2560–2566.

[25] Tian Q, Hu J, Zhu Y, Zou R, Chen Z, Yang S, Li R, Su Q, Han Y and Liu X. Sub-10 nm Fe_3O_4@$Cu_{2-x}S$ core−shell nanoparticles for dual-modal imaging and photothermal therapy. J Am Chem Soc 2013;135:8571−8577.

[26] Choi HS, Liu W, Misra P, Tanaka E, Zimmer JP, Ipe BI, Bawendi MG, Frangioni JV. Renal clearance of quantum dots. Nat Biotechnol 2007;25(10):1165-1170.

[27] Wu MC, Deokar AR, Liao JH, Shih PY, and Ling YC. Graphene-based photothermal agent for rapid and effective killing of bacteria. ACS Nano 2013;7(2):1281–1290.

[28] Yang K, Zhang S, Zhang G, Sun X, Lee ST, and Liu Z. Graphene in mice: ultrahigh in vivo tumor uptake and efficient photothermal therapy. Nano Lett 2010;10:3318–3323.

[29] Robinson JT, Tabakman SM, Liang Y, Wang H, Sanchez Casalongue H, Vinh D and Dai H. Ultrasmall reduced graphene oxide with high near-infrared absorbance for photothermal therapy. J. Am. Chem. Soc. 2011;133;6825-6831.

[30] Yang K, Wan J, Zhang S, Tian B, Zhang Y and Liu Z. The influence of surface chemistry and size of nanoscale graphene oxide on photothermal therapy of cancer using ultra-low laser power. Biomater. 2012;33;2206-2214.

[31] Akhavan O, Ghaderi E and Emamy H. Nontoxic concentrations of PEGylated graphene nanoribbons for selective cáncer cell imaging and photothermal therapy. J. Mater. Chem. 2012;22;20626-20633.

[32] Akhavan O, Ghaderi E, Aghayee S, Fereydooni Y and Talebi A. The use of a glucose-reduced graphene oxide suspension for photothermal cancer therapy. J. Mater. Chem. 2012;22;13773-13781.

[33] Akhavan O and Ghaderi E. Graphene nanomesh promises extremely efficient in vivo photothermal therapy. Small 2013;9;3593-3601.

[34] Shi X, Gong H, Li Y, Wang C, Cheng L, Liu Z. Graphene-based magnetic plasmonicnanocomposite for dual bioimaging and photothermal therapy. Biomaterials 2013;34:4786-4793.

[35] Wang Y, Wang H, Liu D, Song S, Wang X, Zhang H. Graphene oxide covalently grafted upconversion nanoparticles for combined NIR mediated imaging and photothermal/photodynamic cancer therapy. Biomaterials 2013;34:7715-7724.

[36] Smith AM, Mancini MC, Nie S. Bioimaging: second window for in vivo imaging. Nat Nanotechnol 2009;4:710-711.

[37] Li JL, Tang B, Yuan B, Sun L, Wang XG. A review of optical imaging and therapy using nanosized graphene and graphene oxide. Biomaterials 2013;34:9519-9534.

[38] Roper DK, Ahn W. and Hoepfner M. Microscale heat transfer tranduced by surface plasmon resonant gold nanoparticles. J Phys Chem C Nanomater Interfaces 2007;111(9):3636–3641.

[39] Hsu PC, Lin TA, Tsai IS. Numerous single-layer graphene sheets prepared from natural graphite by non-chemical liquid-phase exfoliation. Micro Nano Lett 2014;9(12):922-926.

[40] Rybin M, Pereyaslavtsev A, Vasilieva T, Myasnikov V, Sokolov I, Pavlova A, Obraztsova E, Khomich A, Ralchenko V and Obraztsova E. Efficient nitrogen doping of graphene by plasma treatment. Carbon 2016;96;196-202.

[41] Habash RWY, Bansal R, Krewski D, Alhafid HT. Thermal therapy, part 1: an introduction to thermal therapy. Crit Rev Biomed Eng 2006;34(6):459-489.

[42] Cole JR, Mirin NA, Knight MW, Goodrich GP and Halas NJ. Photothermal efficiencies of nanoshells and nanorods for clinical therapeutic applications. J. Phys. Chem. C 2009;113;12090–12094.

[43] Li B, Wang Q, Zou R, Liu X, Xu K, Lia W and Hu J. Cu7.2S4 nanocrystals: a novel photothermal agent with a 56.7% photothermal conversion efficiency for photothermal therapy of cancer cells. Nanoscale 2014; 6, 3274.

[44] Pattani VP and Tunnell JW. Nanoparticle-mediated photothermal therapy: a comparative study of heating for different particle types. Lasers Surg Med 2012;44:675–684.

[45] Huang P, Lin J, Li W, Rong P, Wang Z, Wang S, Wang X, Sun X, Aronova M, Niu G, Leapman RD, Nie Z and Chen X, Biodegradable gold nanovesicles with an ultrastrong plasmonic coupling effect for photoacoustic imaging and photothermal therapy. Angew. Chem. Int. Ed. 2013;52;13958 –13964.

[46] Cheng FY, Chen CT and Yeh CS. Comparative efficiencies of photothermal destruction of malignant cells using antibody-coated silica@Au nanoshells, hollow Au/Ag nanospheres and Au nanorods, Nanotechnology 2009;20:425104-425113.

[47] Choi J, Yang J, Jang E, Suh JS, Huh YM, Lee K and Haam S. Gold nanostructures as photothermal therapy agent for cancer. Anticancer Agents Med Chem 2011;11:953-964.

[48] Huff TB, Tong L, Zhao Y, Hansen MN, Cheng JX, Wei A. Hyperthermic effects of gold nanorods on tumor cells. Nanomedicine 2007;2(1):125–132.

[49] Link S, El-Sayed MA. Shape and size dependence of radiative, non-radiative and photothermal properties of gold nanocrystals. Int Rev Phys Chem 2000;19:409–453.